J. Mech. Phys. Solids Vol. 39, No. 3, pp. 385–415, 1991.
Printed in Great Britain.

0022–5096/91 $3.00 + 0.00

ON THE TEMPERATURE DISTRIBUTION AT THE VICINITY OF DYNAMICALLY PROPAGATING CRACKS IN 4340 STEEL

ALAN T. ZEHNDER† and ARES J. ROSAKIS

Graduate Aeronautical Laboratories, California Institute of Technology, Pasadena, CA 91125, U.S.A.

(*Received* 22 *September* 1989; *in revised form* 21 *December* 1989)

ABSTRACT

THE HEAT generated due to plastic deformation at the tip of a dynamically propagating crack in a metal causes a large local temperature increase at the crack tip which is expected to affect the selection of failure modes during dynamic fracture and to thus influence the fracture toughness of the material. The distribution of temperature at the tips of dynamically propagating cracks in two heat treatments of AISI 4340 carbon steel was investigated experimentally using an array of eight high speed indium antimonide, infrared detectors. Experiments were performed on wedge loaded, compact tension specimens with initially blunted cracks, producing crack speeds ranging from 1900 to 730 m/s. The measurements provide the spatial distribution of temperature increase near the crack tip on the specimen surface. Temperature increases were as high as 465°C over ambient and the region of intense heating (greater than 100°C temperature rise) covered approximately one third of the active plastic zone on the specimen surface. The observed temperature increase profiles clearly show the three-dimensional nature of the fracture process near the specimen surface and provide valuable information regarding the dynamic formation of shear lips and their role in the dissipation of energy during dynamic crack growth. Preliminary temperature measurements performed on side-grooved specimens are also reported.

INTRODUCTION

KRAFFT and IRWIN (1964) recognized that the heat generated at the tip of a dynamically propagating crack might play a very influential role in determining the dynamic fracture propagation toughness of a material. The source of the crack tip heating during dynamic crack growth in metals is the dissipation of plastic work near the crack tip. TAYLOR and QUINNEY (1934) and others (see BEVER *et al.*, 1973), have shown that most of the energy of plastic deformation (>90%) is dissipated as heat while the remainder is stored in the material in the form of dislocation energy, and energy due to other defects created by the deformation.

Despite the potential importance of crack tip heating on dynamic fracture toughness no attempt to measure directly the temperature at the tip of a truly dynamically growing crack in a metal has yet been made. However, recent advances in infrared detectors now make it possible to measure, in real time, the spatial distribution of

†Current affiliation: Department of Theoretical and Applied Mechanics, Cornell University, Ithaca, NY 14853-1503, U.S.A.

crack tip temperature for dynamically propagating cracks (cracks propagating with velocities higher than 30% of the material shear wave speeds).

The goal of the experiments described in this investigation is to measure directly the amplitude and spatial structure of temperature fields generated at the vicinity of the tips of cracks propagating dynamically in 4340 steel. The experimental results are also used to calculate the distribution of the density of plastic work rate at the vicinity of the propagating crack tips. The concept of the experiments is as follows: a linear array of eight high-speed indium antimonide infrared detectors is used to measure the temperature at eight observation points covering a line segment perpendicular to and intersecting the path of a crack propagating dynamically in a 4340 steel specimen. As the crack traverses the line segment, the voltage outputs from each of the eight detector elements are recorded simultaneously on a set of digital oscilloscopes. At the same time the crack length record is measured using a conductive grid technique. By recording the temperature versus time at the observation points and by using the measured crack length versus time record, the temperature distribution near the crack tip is obtained. This information is valuable in quantifying the role of crack tip heating on fracture toughness, and in determining the distribution of plastic work rate density within the active plastic zone. The eventual goal of this work is to assess the role of the competing phenomena of thermal softening and strain rate hardening on the selection of failure mechanisms during the dynamic fracture of metals.

The spatial resolution of the temperature measurement is fine relative to the crack tip plastic zone and to the resulting plastic wake. The eight detector elements each measure temperature from separate 160-μm square regions, with a 200-μm center-to-center spacing between observation regions. The total length covered is thus 1.56 mm perpendicular to the crack path. Comparison of the above to an estimate of the plastic zone size shows that the spatial resolution of the measurement is approximately 1/12 of the *maximum* plastic zone size.

Consider a mode-I crack propagating dynamically with an instantaneous crack length $a(t)$, and speed $\dot{a}(t)$, as shown in Fig. 1. As the crack approaches a material particle near the $x_2 = 0$ line, the particle is loaded first elastically, and then plastically within the active crack tip plastic zone, defined as the region where the plastic work rate, $\dot{W}^p$, is positive. When the particle exits the active plastic zone, it unloads elastically and enters the wake region. During the initial elastic loading there is a very small thermoelastic cooling due to the volume dilation, followed by heating during the plastic loading. The particle rapidly heats up to its maximum temperature and

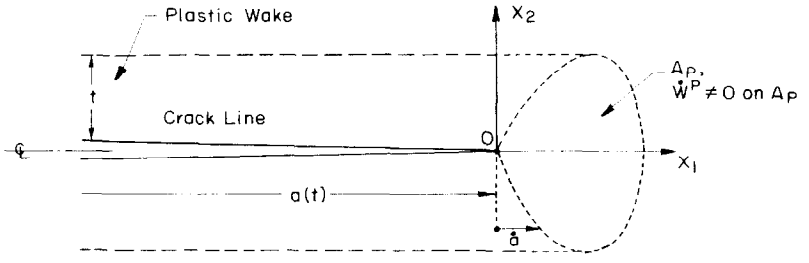

FIG. 1. Active plastic zone and wake for mode-I dynamic crack growth.

then slowly cools down by conduction after the crack passes. The time, t, for the particle to reach its maximum temperature corresponds to the time it takes for the particle to traverse the active plastic zone. In terms of $\dot{a}$ and plastic zone size r_p, this time is roughly equal to $t = r_p/\dot{a} \approx 1.5$ μs, obtained by estimating $r_p \approx 1.5$ mm and $\dot{a} \approx 1$ mm/μs. After the crack passes and the material is in the plastic wake no further heating occurs since $\dot{W}^p = 0$ here.

For an elastic–plastic, isotropic, homogeneous material with constant thermal conductivity, the heat conduction equation can be written as

$$k\nabla^2 T - \alpha(3\lambda + 2\mu)T_0\dot{\varepsilon}^e_{\kappa\kappa} + f\sigma_{ij}\dot{\varepsilon}^p_{ij} = \rho c\dot{T}, \tag{1}$$

where k is the thermal conductivity, T is the temperature, α is the coefficient of thermal expansion, λ and μ are elastic constants, T_0 is the initial temperature, $\dot{\varepsilon}^e_{ij}$, σ_{ij} and $\dot{\varepsilon}^p_{ij}$ are the elastic strain, stress and plastic strain rate tensor components respectively, ρ is the density and c is the specific heat. The quantity f is the fraction of plastic work rate density, $\dot{W}^p = \sigma_{ij}\dot{\varepsilon}^p_{ij}$, dissipated as heat. In general f is not a constant but is a function of plastic strain, strain rate and possibly other variables. However, the experimental data given by TAYLOR and QUINNEY (1934) and in BEVER *et al.* (1973) indicate that f is usually between 0.9 and 1.0. The solution to (1), in terms of T, is given by CARSLAW and JAEGER (1959) and involves integrals of $f\sigma_{ij}\dot{\varepsilon}^p_{ij}$ over time and over the active plastic zone. Thus if the distribution of the plastic work rate density $\dot{W}^p$ is known from an analytical or a numerical model of the crack growth problem, then the temperature distribution around the crack tip can be determined. This is exactly the approach taken by a number of theoretical investigations on the subject, some of which are outlined below.

In the early investigation of RICE and LEVY (1969), the crack tip field is approximated by a Dugdale-type line plastic zone model. The resulting calculation allows the maximum temperature $T_{\max}$ to be calculated given the stress intensity factor, K^d_{I}, the crack speed, the yield stress and the thermal properties of the material. They find that $T_{\max}$ increases with increasing K^d_{I} and increasing $\dot{a}$. For properties typical of mild steel, $T_{\max}$ is approximately 200°C, while for titanium (which has a much lower conductivity) $T_{\max} \approx 500$°C or higher. In WEICHERT and SCHÖNERT (1978), the plastic work rate density is spread uniformly over a circular or rectangular region propagating with the crack tip. By estimating the energy release rate and the area over which the heating occurs, they predict temperature increases well in excess of 3000°C for brittle materials such as glass or quartz.

For dynamic crack growth in viscoplastic materials, SUNG and ACHENBACH (1987) used a plane strain solution to estimate the peak temperature near the crack tip. Their results indicate maximum temperature increases as high as 700°C for a crack propagating at 300 m/s. If this result is accurate, it indicates that crack tip heating is very important, since a temperature increase of 700°C will certainly affect the local mechanical properties of the material.

In finite element calculations for the crack tip temperature rise, KUANG and ATLURI (1985) distributed the heating due to plastic work rate density uniformly and in a $1/r$ distribution, where r is the distance from the crack tip. They estimated $T_{\max} \approx 1000$°C for a crack propagating at high speed. MALALI (1988) used finite elements to solve for $\dot{W}^p$ for mode-III (antiplane shear) dynamic crack growth in an elastic–perfectly

plastic material. In this solution $T_{max} \approx 240$ C for steel and is approximately 4000 C for a titanium alloy.

A recent finite element calculation by KRISHNAKUMAR *et al.* (1989) simulated plane strain, steady state, dynamic crack growth in a viscoplastic material. Using the plastic work rate distribution calculated from the finite element model, and assuming that all of the work is dissipated as heat, they calculated the resulting temperature rise near the crack tip. The results indicate that the maximum crack tip temperature increase is 160 C to 240 C, depending on crack growth speed and on material properties.

Care must be taken in interpreting any of the above results since they are very sensitive to the assumptions of the model, to the constitutive law, to whether the calculation assumes plane strain, plane stress or antiplane shear kinematics, and to the choice of material parameters, which are not always realistic. For example it is unlikely that a ductile steel with a low yield stress can sustain crack growth at speeds of 1000 m/s, as assumed in some analyses. Work in progress by DENG and ROSAKIS (1989), who are numerically modelling *plane stress*, mode-I crack growth in high strength steel, should provide numerical estimates that can more readily be compared with *surface* experimental measurements.

From the experimental viewpoint, several authors have used infrared (IR) detectors to study problems in solid mechanics. A copper-doped germanium detector was used by MOSS and POND (1975) to study the heat generated by discontinuous yielding in copper. In their experiment radiation was focused onto the detector with a spherical mirror system and the resulting signals were recorded dynamically. Since a single element detector was used, no attempt was made to produce a full-field image of the temperature field.

The first experiments to use a focused, imaging system of IR detectors for a truly dynamic experiment are those of Duffy and co-workers (DUFFY, 1984; HARTLEY *et al.*, 1987). They used a linear array of indium antimonide (InSb) detectors focused on a specimen undergoing dynamic shear loading. The dynamic shear band formed in their experiments is a source of heat causing the temperature to rise 400 C in 50 μs. It was found that this heating is critical in producing thermal softening, leading to deformation instability.

IR detectors have even been used to study stress wave reflections, by measuring the very small temperature changes produced by the thermoelastic effect in stress waves (MONCHALIN, 1984). In this work a low-speed, pyroelectric, thermal detector was employed. Thermal cameras, which typically scan their field of view in 1/30 second, have been used in numerous quasi-static experiments. For example, thermal cameras are applied for a stress analysis technique known as SPATE (BAKER and OLIVER, 1986) (Stress Pattern Analysis by Thermal Emissions) that measures the temperature due to the thermoelastic heating and cooling of a body under cyclic loading. Unfortunately such systems are too slow for applications involving truly dynamic phenomena.

Most of the experimental measurements of temperature in truly dynamic fracture (crack velocities above 30% of the shear wave speeds) have concentrated on measuring the energy release rate or the maximum temperature at the crack tip. In the work by FULLER *et al.* (1975), a number of experimental techniques were combined to study

crack tip heating. A single element, unfocused, IR detector system was used to measure the maximum temperature at the tip of a dynamic crack in PMMA. The maximum temperature recorded was 500°C. In addition, thermocouples and a liquid crystal film deposited on the specimen surface were employed to estimate the total heat dissipated during crack growth.

In the work by WEICHERT and SCHÖNERT (1978), an unfocused, high speed, infrared spectrometer was used to measure peak temperature during the fragmentation of a glass plate. In addition, they used thermistors to estimate total heat generation during crack growth.

In recent work by SHOCKEY *et al.* (1983), thermocouples of 25–50 μm dimensions are welded to the surface of the high-strength steel specimen near the prospective crack path. As the crack propagates past the thermocouples the temperature is recorded. Typically the temperatures measured are less than 1°C since the thermocouples are located greater than 1 mm from the crack path, where the heating actually occurred. By treating the crack as a one-dimensional heat source that instantaneously delivers a heat flux all along the crack line at the same time, the magnitude of this heat flux can be computed from the measured temperature. In this way an estimate of the energy release rate, G, can be obtained. Values obtained in SHOCKEY *et al.* (1983) for G are within a factor of 2 of the value obtained from $G \approx K_I^2/E$, where K_I is the stress intensity factor and E is Young's modulus.

Other experimental measurements of near tip temperatures are presented by DÖLL (1973), TOMASHEVSKII *et al.* (1975), and FOX and SORIA-RUIZ (1970). A metallurgical study presenting evidence of local melting during the fracture of two titanium alloys is presented in BRYANT *et al.* (1986).

All of the above studies make use of brittle materials such as glass, quartz and PMMA or very high strength steel, and concentrate on measuring either the maximum temperature or the total energy dissipated as heat. An exception to the above are the recent results by KLEMM (1989), who studied fast crack growth in highly ductile pipeline steels (crack velocities up to 80 m/s). By using a series of thermocouples he obtains the temperature profile across the large, 50-mm radius, plastic zone and records maximum temperature increases of the order of 100°C. He then uses the experimental measurements to estimate the energy expended during crack growth.

In the experiments described here, we use an array of focussed IR detectors to study the *spatial distribution* of temperature increase within the plastic zone of a crack propagating dynamically (speeds of the order of 30–60% of the shear wave speed) in 4340 steel. The experimental set-up is very similar to that developed by Duffy and co-workers (DUFFY, 1984; HARTLEY *et al.*, 1987) for studying dynamic shear bands. In addition, we use our temperature measurements to obtain the distribution of plastic work rate ahead of the crack tip and to study the dynamic formation of shear lips and their role in the dissipation of energy during dynamic crack growth.

DESCRIPTION OF EXPERIMENTS

Electromagnetic radiation is constantly emitted from bodies that are at temperatures greater than absolute zero. Since the radiation intensity increases as θ^4,

where θ is the absolute temperature of the body, measurement of radiation can provide a sensitive measurement of temperature. This is the central concept of the experiment described here. As the crack propagates, it heats up the material near the crack tip, emitting infrared radiation from the specimen surface. The emitted radiation is measured along a line perpendicular to the crack path, and the temperature around the crack tip is determined by applying a calibration of temperature versus measured radiation.

SPECIMENS

The specimens used for this experiment were wedge-loaded compact tension specimens of 4340 steel with the dimensions shown in Fig. 2. The mechanical and thermal properties and chemical composition are given in Table 1. Note that two different heat treatments were tested in these experiments.

The wedge loaded compact tension geometry was chosen because the compressive stress induced by the wedge stabilizes the crack path and ensures straight crack growth. This is very important in such experiments, since the detectors can measure across a distance of only 1.5 mm; thus the crack must propagate within 0.75 mm of the desired path in order for an experiment to be successful. The specimens were prepared by grinding, lapping and then polishing the specimen surfaces with a 9 μm diamond paste. Several specimens had side grooves machined along the crack paths. Two geometries were used, a semicircular groove of radius 1.5 mm, and a V-notch groove of width 3 mm and depth 1.5 mm.

An array of lines of conductive paint spaced 3 mm apart was silkscreened onto the back of each specimen, using techniques developed by HUDAK *et al.* (1987). These strips are visible on the back of the specimen pictured in Fig. 3. As the crack runs,

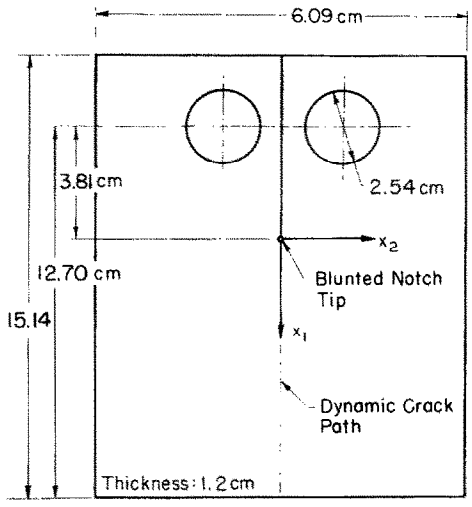

FIG. 2. The wedge loaded compact tension specimen.

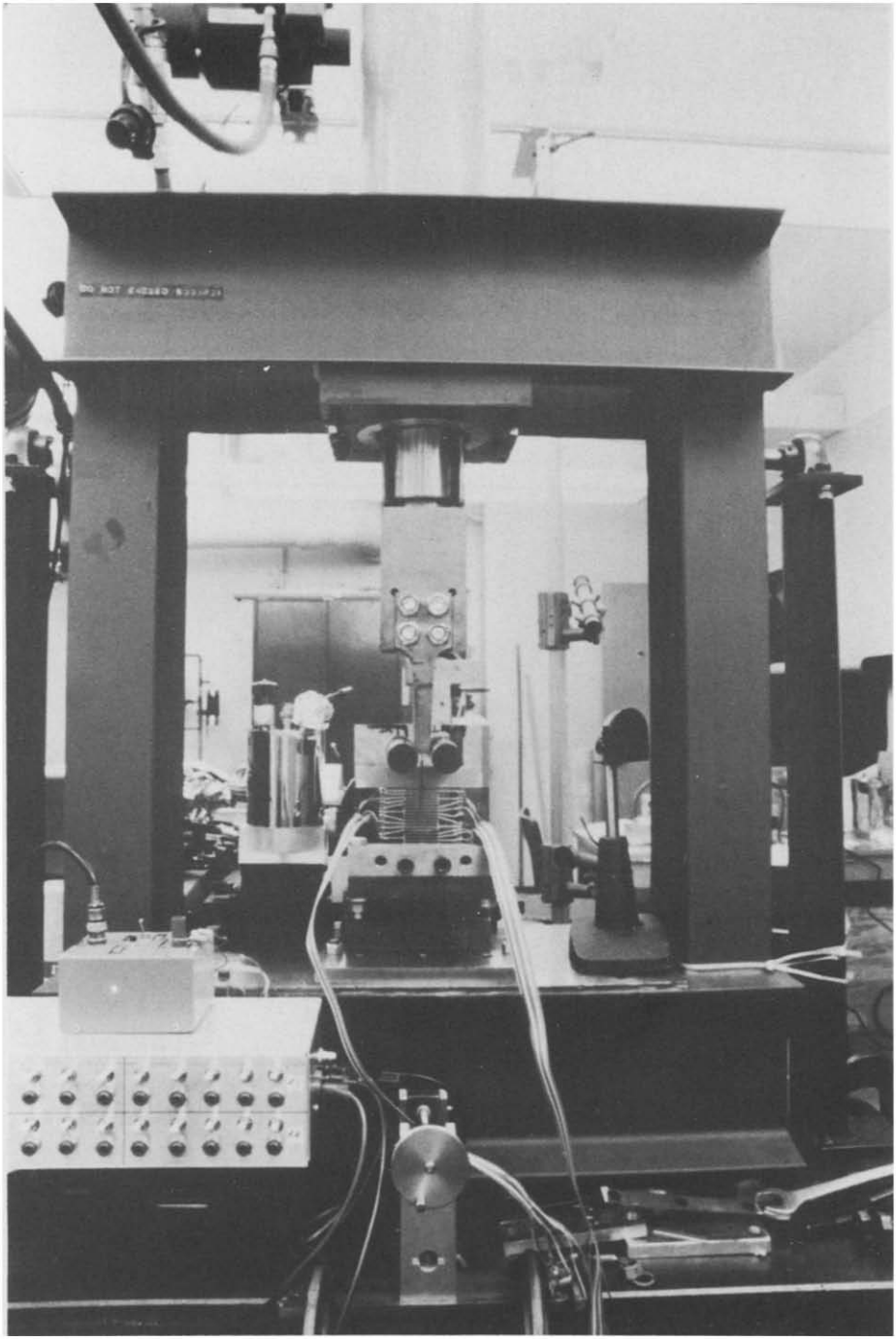

FIG. 3. Photograph of loading frame mounted on optical table, loading wedge, test specimen and conductive strips for velocity measurement.

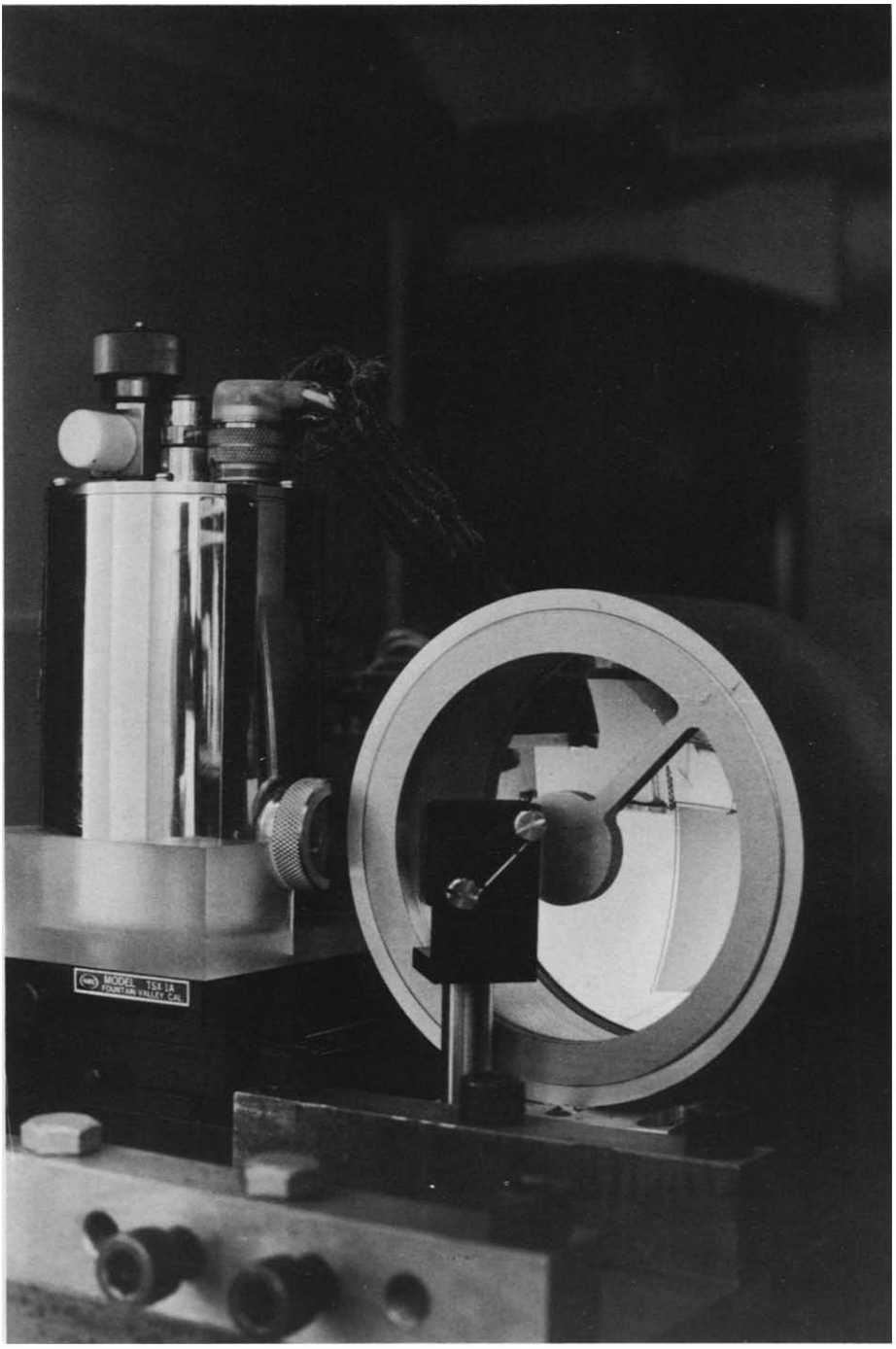

FIG. 5. Photograph of IR detector dewar and mirrors.

TABLE 1. *Mechanical and thermal properties and chemical composition* 4340 *steel, aircraft quality, vacuum degassed*

Heat treatment	σ_0 (MPa)	K_{Ic} (MPa$\sqrt{m}$)	Hardness, HRC
"Quenched and tempered" 871°C 1 h, air cool 843°C 1½h, oil quench 316°C 1 h, air cool	1490†	50†	44–45
"Oil quenched" 871°C 1 h, air cool 843°C 1½ h, oil quench	1700‡	44‡	49–55

Chemical composition, %

C	Mn	P	S	Si	Cu	Ni	Cr	Mo	Sn	Al	Fe
0.42	0.71	0.007	0.013	0.23	0.12	1.78	0.83	0.25	0.005	0.033	Balance

Properties at 0°C:‡	
Thermal conductivity	$k = 34.6$ W/m-K
Thermal expansion	$a = 11.2 \times 10^{-6}$ K^{-1}
Specific heat	$c = 448.0$ J/kg-K
density	$\rho = 7834$ kg/m^3
Thermal diffusivity	$\alpha = 0.99 \times 10^{-5}$ m^2/s

†Source: ZEHNDER and ROSAKIS (1989).

‡Source: *Aerospace Structural Metals Handbook*, Metals and Ceramics Information Center, Battelle Columbus Laboratories, Columbus, Ohio, 1989.

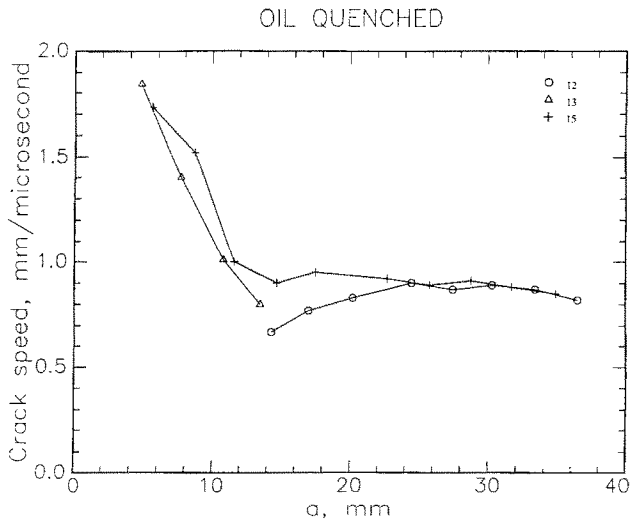

FIG. 4. Crack speed vs crack length for oil-quenched specimens.

the conductive strips are broken and the resistance of the entire array is increased. Thus a time record of the resistance (measured with a bridge circuit) provides the time history of the crack motion. This technique has been shown to be very reliable for applications to high strength steel. The crack length record is differentiated using the incremental polynomial fit method described by ZEHNDER and ROSAKIS (1989). Typical crack speed records are shown in Fig. 4 for oil-quenched specimens containing an initial crack tip diameter of 1 mm. It is seen that the crack speed, $\dot{a}(a)$, is highly repeatable and remains nearly constant over a substantial portion of the specimen.

The specimens were loaded by a hydraulic cylinder mounted in a steel frame that rests on an optical table, as shown in Fig. 3. The wedge is driven slowly between the loading pins until a sharp crack initiates from the initially blunted notch tip. Due to the geometry of the loading and the initial bluntness of the notch, the resulting crack propagates unstably at high speeds ranging from 1900–1000 m/s, depending on the initial bluntness.

INFRARED DETECTORS

Based on the analytical results summarized in the introduction, the maximum crack tip temperature increases were anticipated to be in the range of 100–1000° C. At such temperatures the emitted infrared radiation is primarily in the 1–2 μm wavelength range. In addition, rise times for the temperatures were expected to be in the 1–2 μs range.

Our choice of indium antimonide (InSb), infrared (IR) detectors was dictated by the wavelength and rise time requirements described above. These detectors are sensitive to radiation with wavelengths from 1–5.5 μm. The particular system chosen consists of eight 0.16 mm × 0.16 mm InSb detector elements in a linear array with a center-to-center spacing of 0.20 mm. The array is mounted in a liquid nitrogen (LN2) dewar to cool the detectors to 77 K, thus minimizing their electrical noise and maximizing their sensitivity. The LN2 dewar is clearly visible in the photograph of Fig. 5 and is sketched in Fig. 6. The detectors are located behind the sapphire window in the dewar.

Each detector is connected to its own amplifier and the amplified signals are recorded on separate high speed digital oscilloscopes, at a 2-MHz sampling rate. The frequency response of the system of detectors and their amplifiers is from 4–300 kHz. The 4 Hz lower limit means that the system is not affected by low frequency background radiation. The 300 kHz upper limit corresponds to a minimum detectable rise time of 0.75 μs, well below the anticipated 1–2 μs rise times. The bandwidth of this system is a compromise between speed and signal to noise ratio. The capacitance of a detector element is proportional to the detector area, thus higher speeds can be achieved by reducing the detector area. However, some sensitivity will be sacrificed since less radiation is collected on a smaller element.

The responsivity of the system used here is on the order of 10^8 V/W, and the maximum output signal is approximately 15 V. In order to avoid saturating the system, the amount of radiation incident on the detectors was limited by placing a small aperture in the optical system.

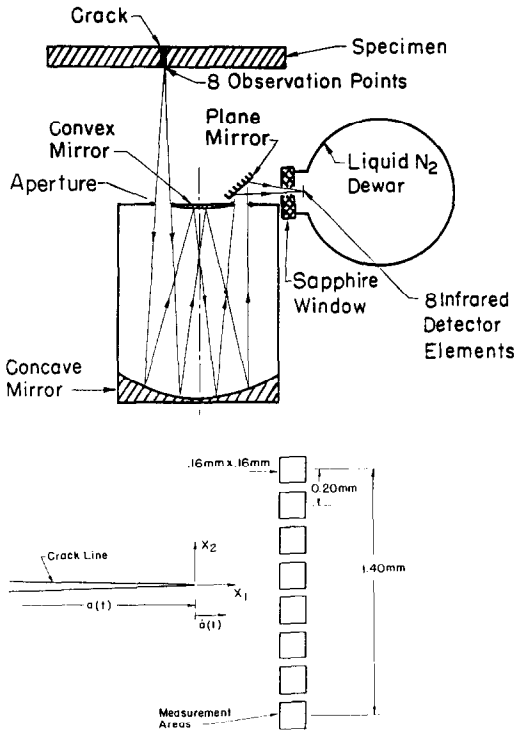

FIG. 6. Schematic of focusing optics and of points on test specimen from which temperature is measured.

It was found that temperature increases as low as 20°C could be detected. However, when the temperature increase was less than approximately 50°C, the signal-to-noise ratio was on the order of one. Thus accurate data could not be obtained from surfaces at temperatures below 50°C above ambient.

INFRARED OPTICS

To measure the crack tip temperature distribution, the infrared radiation must be imaged from the eight areas on the specimen surface onto eight elements of the detector array. The optical system illustrated in Fig. 6, and also seen in Fig. 5, consists of two spherical mirrors and a plane mirror, and was used to focus radiation onto the detectors. The magnification of the optical system is one, and thus the size and spacing of the areas of measurement are equal to that of the detectors. As shown in Fig. 6, the size of the measurement areas is 160×160 μm, the center-to-center spacing is 200 μm while the total length covered is 1.56 mm.

Initial optical alignment was performed by installing a Plexiglas replica of the actual specimen in the specimen holder. A laser beam was aimed through the Plexiglas replica, perpendicular to the replica surface and passing through the region on the

specimen where it is desired to measure the temperature. The optical system was adjusted so that the laser beam passed perpendicularly through the center of the aperture and onto the center of the detectors. To aid in focusing, a 10 lines/mm crossed diffraction grating was taped onto the replica and the grating was illuminated. Fine focusing was performed by adjusting the optics until the image of the grating on the detector elements was sharp.

To align the detectors such that they intersect the prospective crack line, a 0.10 mm diameter wire was carefully taped to the actual specimen along the prospective crack path. The specimen was then put in place in the loading frame. The wire was electrically heated and the system was aligned so that the radiation from the wire was sensed on one of the central elements.

The heated wire has a diameter less than the size of the detector elements, thus ideally, radiation from the wire should be detected on one element only and not on the neighboring elements. However, crosstalk that is intrinsic to the closely spaced detector array and is also due to optical aberrations will produce a small signal on the neighboring elements. It was found that crosstalk was approximately 7%. A procedure was developed to account for the crosstalk by assuming that the signal produced by an element is composed of contributions from that element plus 7% of the signal from its closest neighbors.

CALIBRATION

Careful calibration of the system is crucial for obtaining accurate results. The voltage output, V, of a detector is given by

$$V(T) = A_r \int_{1\,\mu m}^{5.5\,\mu m} P(\lambda, T) R(\lambda)\, d\lambda, \tag{2}$$

where A_r is the amplifier gain, $R(\lambda)$ is the spectral responsivity of the detector and $P(\lambda, T)$ is the radiant power falling on the detector, given by

$$P(\lambda, T) = \beta \cdot A \cdot \varepsilon(\lambda, T) \frac{C_1}{\lambda^5 (e^{C_2/\lambda T} - 1)},$$

where A is the detector area, β is the fraction of radiation emitted from the specimen that is transmitted to the detectors, $\varepsilon(\lambda, T)$ is the emissivity of the specimen at wavelength λ and temperature T, and C_1 and C_2 are constants of the Planck radiation function, $C_1 = 37404$ W $(\mu m)^4/cm^2$, $C_2 = 14387$ μm-K.

Unfortunately it is difficult to accurately measure $\varepsilon(\lambda, T)$, β and $R(\lambda)$. Thus an experimental calibration that lumps all these parameters together and provides a direct relationship between V and T was performed. The procedure was to heat a sample of the 4340 steel, with the same surface finish as the actual test specimens, in a furnace. When the heated sample was removed from the furnace, it was placed in front of the optical system such that it was in focus. As the sample cools the voltage output from the detectors and the sample temperature (measured with a thermocouple) were simultaneously recorded. The radiation was chopped at 1000 Hz by

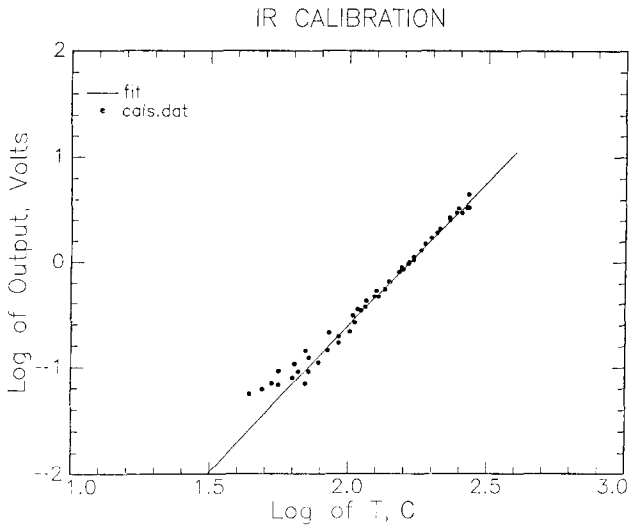

FIG. 7. Calibration of IR detectors. Voltage versus specimen temperature on log–log scale for ungrooved specimens.

placing a rotating disk containing holes around its perimeter into the optical path. It is necessary to introduce high-frequency components into the signal since the amplifiers do not amplify signals below 4 Hz. The calibration data was plotted on a log–log scale as shown in Fig. 7. It is seen that the data falls onto a straight line. Evaluation of (2) using values of $\varepsilon(\lambda, T)$, β, $R(\lambda)$ collected from reference books also shows a linear relation between voltage and temperature increase in a log–log scale.

Note that separate calibrations were performed for the notched specimens since inside the notches the surface finish and hence the emissivity was different. The calibration procedure was repeated for each of the detectors separately. Roughening of the specimen surface due to plastic deformation at the crack tip will also change the emissivity. This effect was investigated by HARTLEY *et al.* (1987) in connection to experiments designed to measure temperature increases due to dynamic shear-band formation. They showed that it is negligible for most of the temperature range.

EXPERIMENTAL RESULTS

Figure 8 shows the time record of the voltage output of each of the eight detector elements, as a crack approaches and passes through the detector points in specimen number 9. Time $t = 0$ corresponds to triggering of the oscilloscopes. The material used in this experiment was an oil-quenched 4340 steel whose material characteristics appear in Table 1. For this experiment and for this particular measurement location, the crack tip speed was found to be approximately constant and equal to 900 m/s (see right-hand section of Fig. 4). The maximum voltage increase was recorded by element 4 (ch4.out in the figure). As is clear from the time record corresponding to this

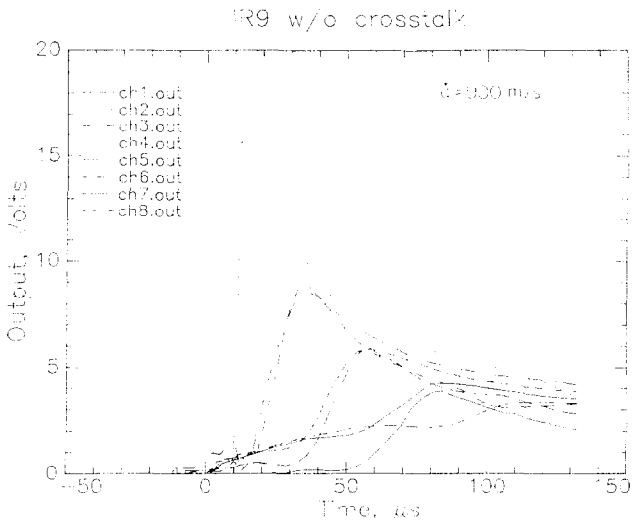

FIG. 8. Specimen 9, oil-quenched steel, IR detector output. Voltage vs time for each element.

channel, the voltage increases rapidly from an almost zero value (from within the noise level of the system) to a maximum value of 16.5 V in approximately 2 μs. This rise time is substantially longer than the 0.75 μs minimum rise time that can be accurately detected by the detector-amplifier.

The voltage output time histories were converted into temperature histories by means of the calibration relation shown in Fig. 7. Since this relation is nonlinear, the resulting temperature records, shown here in Fig. 9, assume a slightly different shape

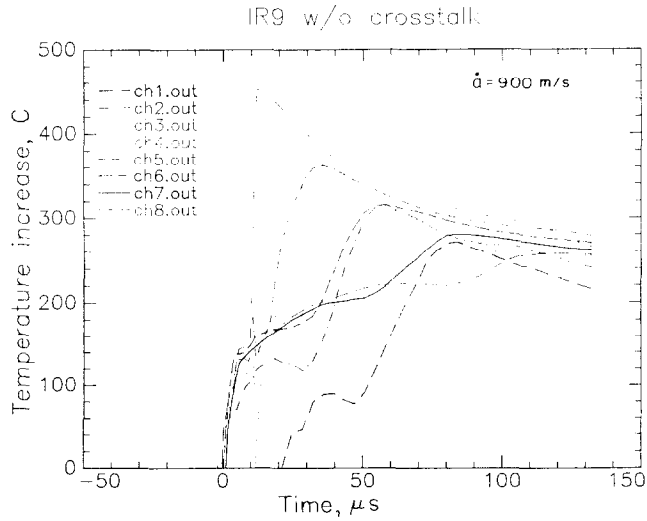

FIG. 9. Specimen 9, temperature increase over ambient vs rise time for each element.

than the voltage records, but nevertheless retain the basic characteristics of Fig. 8. In this experiment the crack tip traversed the array of detection points slightly off center, but through the region focused on element 4. This element recorded a maximum temperature increase of 450°C while the rise time was 2 μs. As may be expected by local symmetry, the elements to the left and right of element 4 (channels 3 and 5) recorded temperature increases which are very similar to each other. These elements also had markedly slower rise times than element 4.

Two alternative ways of viewing these results are shown in Figs 10 and 11. These figures show contours of equal temperature increase near the propagating crack tip. The contours were obtained from the temperature increase versus time results of Fig. 9, by converting the time axis into distance parallel to the direction of crack growth, using the measured crack tip speed of 900 m/s and assuming that the crack propagates with a constant velocity. Although this is clearly a simplifying assumption, its appropriateness is justified by the velocity history data presented in Fig. 4 at least for observation distances greater than 12 mm from the tip of the initial notch.

In both Figs 10 and 11 the estimated crack tip position is at $x_1 \simeq -0.5$ mm, $x_2 \simeq 0.6$ mm. The length scales of Fig. 10 show that this figure corresponds to a *close-up* view of temperature increase in the near vicinity of the propagating crack. The isotherms of Fig. 10 clearly show that intense heating (temperatures ranging from 450–150°C) extends in a narrow region approximately 1 mm ahead of the crack tip, while the half width of the resulting wake of temperatures is approximately 0.25 mm. It should be observed that the isotherms in the wake region behind the crack tip remain almost parallel to the crack line for at least 1.5 mm, suggesting that *locally* the deformation remains essentially adiabatic (i.e. no substantial cooling by conduction is observed in this scale).

The scale of observation of Fig. 11 is very different. Here we present contours of

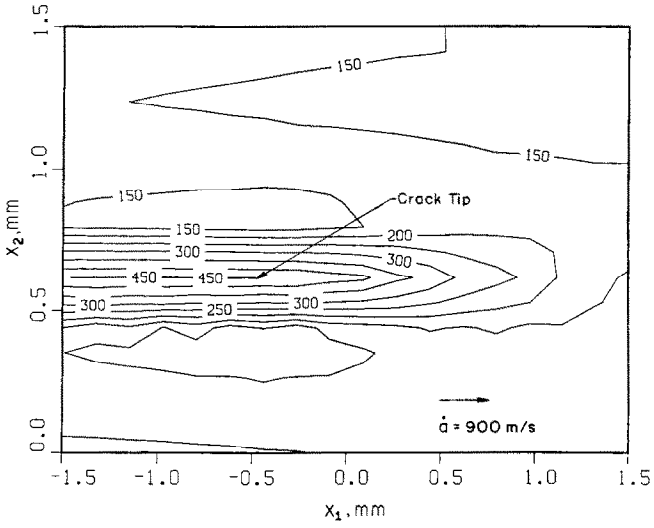

FIG. 10. Specimen 9, contours of equal temperature rise very near the crack tip. Increment between contours is 25°C.

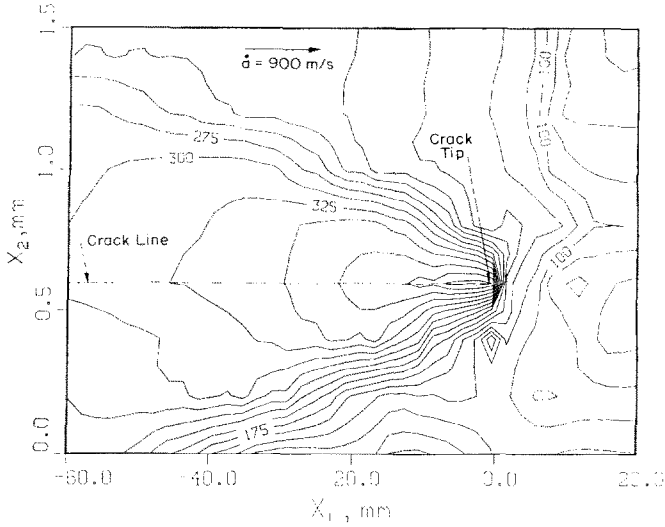

FIG. 11. Specimen 9, contours of temperature increase over ambient in the region away from the crack tip.

temperature increase for distances behind the crack tip as large as 60 mm. The effect of cooling by conduction is apparent by the divergence of the isotherms behind the crack tip. An alternate representation of these results is presented in Fig. 12. This figure is a three-dimensional representation of the temperature distribution near the crack tip. The crack is propagating along the positive x_1 axis (direction of the arrow)

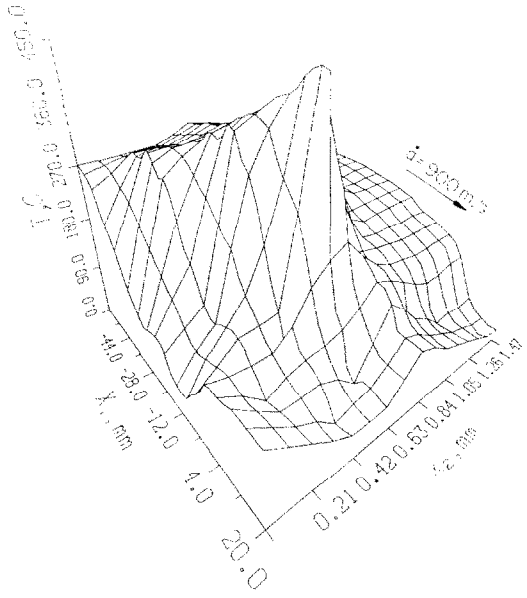

FIG. 12. Specimen 9, surface plot of crack tip temperature distribution.

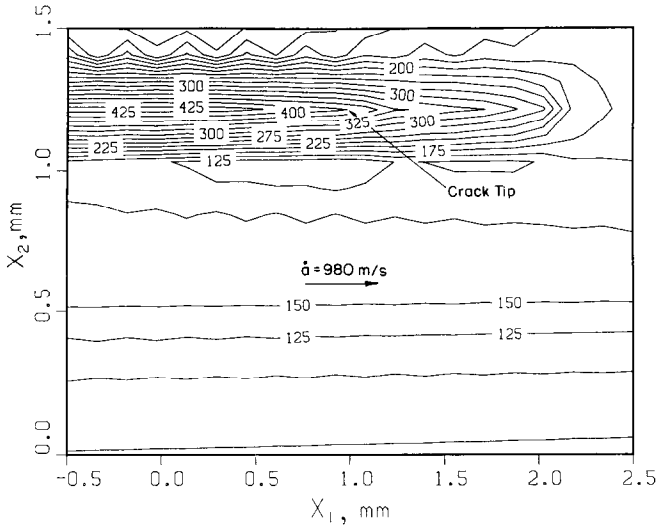

FIG. 13. Specimen 5 (quenched and tempered steel), contours of temperature increase near crack tip.

while the observation points are situated at discrete locations along the x_2 axis. The vertical axis denotes temperature increase in °C. The figure shows the dramatic increase of temperature as the crack tip approaches the points of observation and the slow cooling trend observed after the crack has gone by.

It should be re-emphasized that the measurements are performed over small but nevertheless finite areas (see Fig. 6) and that the above contours have been obtained by assigning the recorded temperature history to the center of these areas. It should therefore be recognized that a certain amount of averaging is involved in this measurement. Nevertheless it is expected that the small size of the measurement allows for the accurate investigation of the general structure of the temperature distribution near the tip. Nonetheless, this averaging makes the recorded *maximum* temperature increase a lower bound to the actual maximum temperature increase at the crack tip.

Figure 13 and 14 show contours of equal temperature increase at the vicinity of a crack in an oil-quenched and tempered 4340 steel specimen (specimen 5). The crack tip velocity was 980 m/s and the crack traversed the array of observation points off-center. Comparison between Figs 10 and 13, and 11 and 14, shows a very similar structure in temperature distribution for these two heat treatments. Comparison between all the experiments conducted on the oil-quenched and the oil-quenched and tempered steels (see Table 1 for mechanical properties) reveals only slight differences in maximum temperature increases for similar velocity. The general trend observed is that maximum temperatures corresponding to the more brittle oil-quenched steel are up to 10°C higher than those recorded for the other heat treatment.

EFFECTS OF SHEAR-LIP FORMATION ON TEMPERATURE

In the experimental results of Fig. 10, the crack traversed the array of observation points near the center. This was not always possible to achieve given the net length

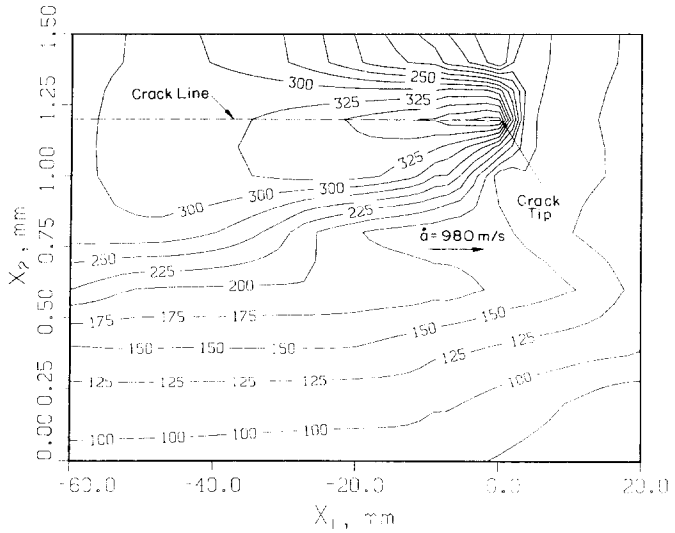

FIG. 14. Specimen 5, contours of temperature increase in the region away from the crack tip.

of the array of observation points (total length of 1.56 mm perpendicular to the prospective crack path) and the fact that it was not always possible to create a perfectly straight crack to within such a small tolerance.

Figure 15(a) shows the spatial distribution of temperature for the case of cracks that traversed the array of observation points near the array end. In this case (specimen 12) the maximum temperature increase was recorded by the end element, number 8, located at $x_2 = 1.4$ mm in the figure. This element shows the most dramatic increase of temperature ahead of the tip and records a temperature peak of 415°C. Perhaps the most interesting feature of this figure is the ridge of local temperature increase shown along the line $x_2 = 0$ farthest away from the crack line. This local temperature increase occurs at points approximately 1.4 mm away from the crack line and was consistently observed in a number of experiments. [See also Fig. 15(b).]

The existence of a local maximum in temperature always occurring at a consistent distance away from the crack line is explained if one takes a close look at the fracture surface of the specimen shown in Fig. 16. The photograph clearly reveals a flat fracture surface in the specimen interior while a shear lip is evident near the specimen surface. The wake of residual plastic deformations is also shown on the specimen surface in the form of a strip of out of plane deformation (local dimpling) along the crack path. The width of this strip was found to be approximately equal to 1.4 mm, which is slightly smaller than the net length of our line of observation points. In addition, the width of this strip is equal to the distance between the crack and the ridge of temperature increase shown in Fig. 15(a) and (b). This is illustrated in the schematic of Fig. 17. This figure shows a thickness cross-section of the specimen, the fracture surface in the specimen interior, and the shear lips near the specimen surface. The eight dots that appear on the specimen surface represent the eight temperature measurement

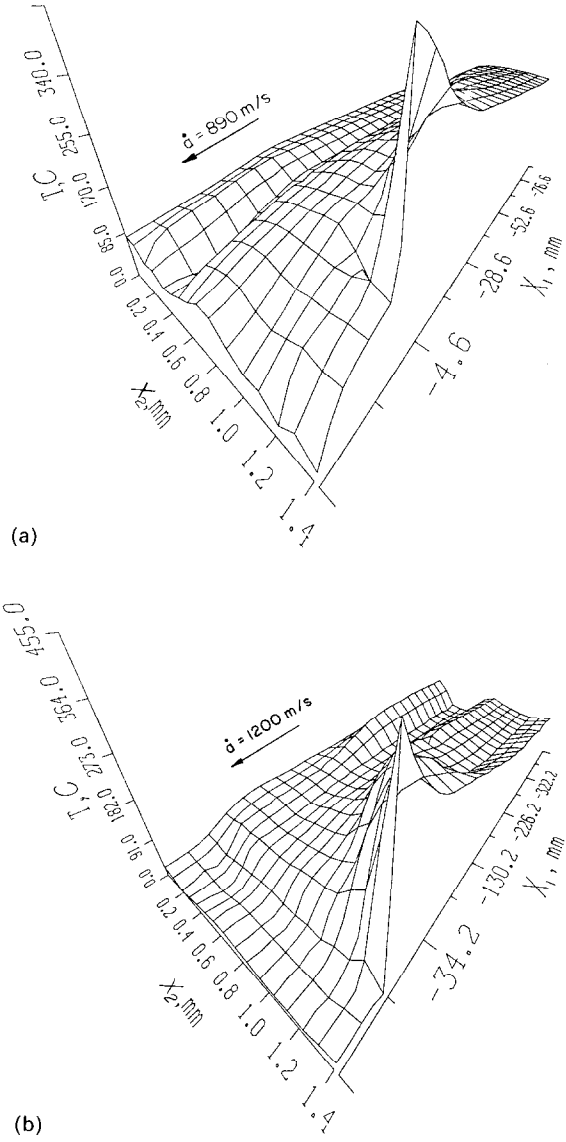

FIG. 15. Surface plots of temperature increase showing major peak due to crack tip and secondary peak due to the 45° shear band corresponding to the opposite side of shear lip. (a) Specimen 12. (b) Specimen 17.

locations. In the specimen interior the crack surface is flat and lies on the plane $x_2 = 0$ while on the specimen surface shear lips are shown.

The process of the creation of shear lips involves some amount of crack tip tunneling followed by the formation of two symmetric 45° shear bands (solid and dotted lines), one of which ruptures (solid line) to produce the 45° crack observed on the specimen

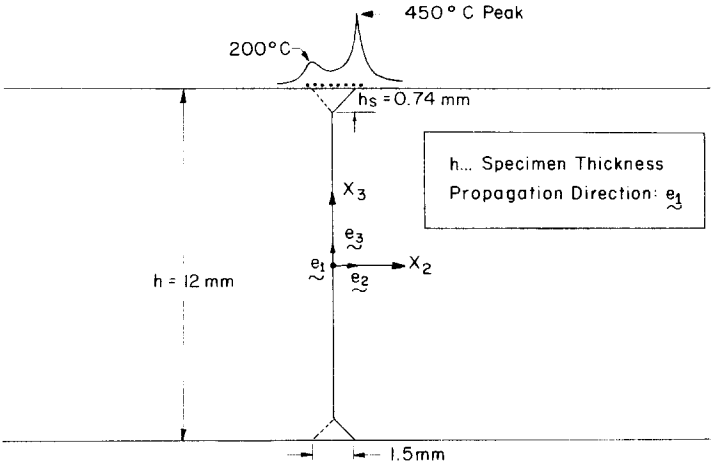

FIG. 17. Schematic of the thickness cross section of the specimen illustrating the formation of shear lips and the associated temperature distribution on the free surface.

surface. The major peak of temperature increase (see Fig. 15) corresponds to the tip of the crack while the minor peak lies exactly at the location where the other 45° shear band (dotted line) meets the specimen surface.

Further evidence of the existence of the ridge of temperatures associated with the 45° shear band is given in the experimental result shown in Fig. 18. To investigate heating due to the formation of the shear band alone, the infrared system was focused slightly off center in this experiment. The temperature increase recorded here is on the order of 200°C and is well above the noise level of our recording system.

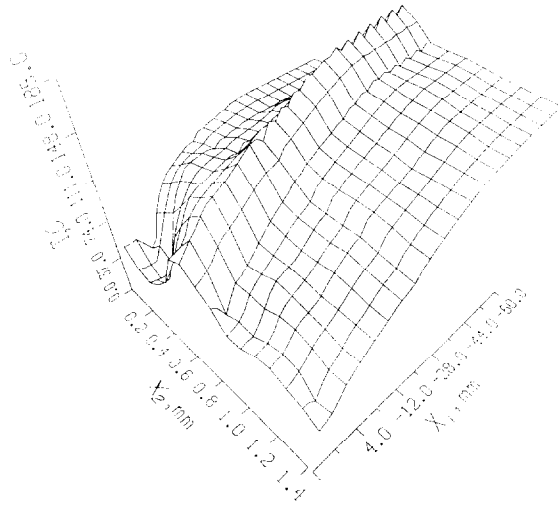

FIG. 18. Specimen 7. Surface plot of temperature showing ridge of temperature due to opposite side of shear lip (45° shear band).

FIG. 16. Photograph of fracture surface and shear lips.

Figures 15 and 18 show that the temperature measurements reflect the highly three-dimensional nature of the rupture process on the specimen surface.

Finally it should be emphasized here that the measurements described above reveal temperature fields strictly on the specimen surface. The very short time scales involved in this measurement ensure that conduction from the specimen interior has no time to affect the temperature recorded on the surface at the vicinity of the dynamically propagating crack. A simple calculation based on known values for the thermal conductivity of 4340 steel reveals that in the time scales of this measurement, the temperature on the specimen surface is only affected by points of the interior lying within distances of less than 30 μm below the specimen surface. In addition, the time scales involved preclude the possibility of any cooling effects due to convection or radiation during dynamic growth.

Specimens with Side Grooves

The results presented in the previous section provide a very accurate account of the temperature field on the specimen surface. These temperature increases are dominated by the complex process of the dynamic formation of shear lips which involves the simultaneous formation of dynamic shear bands and cracks intersecting the surface at 45°. However, in order to obtain some idea of the temperature rise in the specimen's interior, a preliminary series of experiments was performed with side-grooved specimen surfaces. The side grooving was designed to diminish the effect of shear lips and to provide conditions that would at least approximate plane strain like crack tip field constraints in the specimen interior. Two types of side-grooves, V-notched (width 3 mm and depth 1.5 mm) and circularly notched (radius 1.5 mm), were machined along the prospective crack paths shown. Figure 19 shows a set of temperature vs time

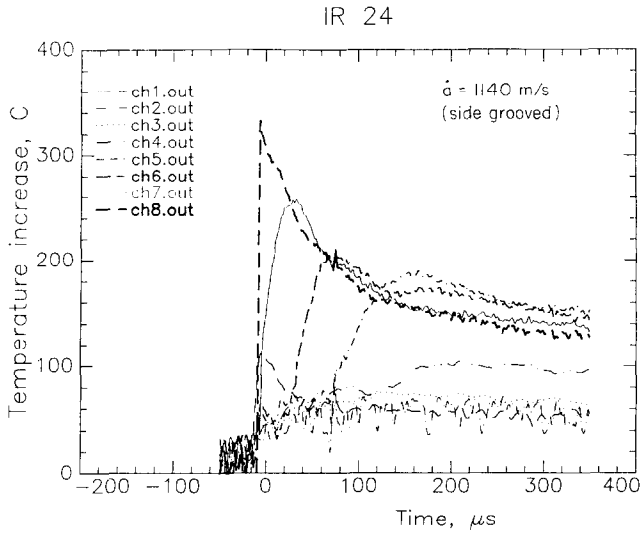

Fig. 19. Specimen 24 (circular groove). Temperature rise vs time for each detector element.

TABLE 2. *Summary of experiments*

Specimen	Heat treatment	a (mm)	$\dot{a}$ (m/s)	T_{max} (°C)	Notes
1	tempered	29	730	410	
5	tempered	29	980	415	
7	oil quenched	14	950	185	shear band temperature
9	oil quenched	14	900	450	
12	oil quenched	25	890	425	
13	oil quenched	8	1300	410	
17	oil quenched	8	1200	465	focused in circular groove
21	oil quenched	8	1100	$\geqslant 420$	voltage went off scale
22	tempered	8	1900	290	focused in V-notch
24	tempered	8	1140	330	focused in circular groove

records corresponding to the circularly notched specimen number 24. These measurements are conducted by focusing the eight detector elements inside the side grooves. A separate calibration was performed to account for the difference in surface roughness due to the machining of the grooves, and to account for possible variations due to the side groove geometries. Due to the small aperture used, the large depth of field of the optical system allows us to focus simultaneously at any level inside the side groove. Our preliminary experiments indicate that the use of side grooves diminishes the size of the resulting shear lips and in addition results in peak temperatures which are up to 20% lower than those recorded by the corresponding measurements on the specimen surface (see Table 2). This reduction may be attributed to differences in the near tip constraints between notched and unnotched geometries.

DISCUSSION OF RESULTS

Plastic work rate density

The distribution of plastic work rate density near the crack tip can be obtained by straightforward differentiation of the temperature field. Assuming that the heating due to plastic work is much higher than the thermoelastic effects and treating the crack growth as *steady state*, (1) can be written as

$$f\sigma_{ij}\dot{\varepsilon}_{ij}^{p} = -\rho c\dot{a}\frac{\partial T}{\partial x_1} - k\nabla^2 T \tag{3}$$

with respect to a coordinate system translating with the crack tip, where x_1 is the direction of crack growth. Note that the conduction term with the crack tip, $k\nabla^2 T$, in (3), involves derivatives of T with respect to x_3, while the measurement provides only $T(x_1, x_2, x_3 = h/2)$, where h is the specimen thickness.

The very short time scales of this measurement (2–10 μs) ensure that convection and radiation heat losses from the surface are very small. In addition, as discussed in the previous section, conduction of heat from the interior of the specimen has no time to affect the surface temperature near the crack tip. As a result, the variation of T

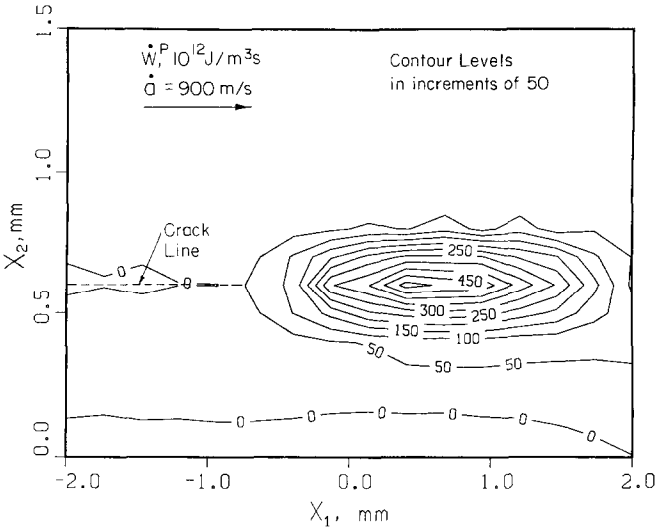

FIG. 20. Specimen 9. Contours of plastic work rate density near crack tip. Increment between contours is 50×10^{12} J/m^3-s.

with respect to x_3 is expected to be small, and little error is incurred by neglecting the $\partial^2 T/\partial x_3^2$ term in (3). Indeed when differentiating $T(x_1, x_2, x_3 = h/2)$ the entire conduction term was found to be small relative to the adiabatic heating term, $-\rho c\dot{a}(\partial T/\partial x_1)$. For distances from the crack tip of less than 3 mm, the ratio $\rho c\dot{a}(\partial T/\partial x_1)/k\nabla^2 T$ was approximately 10^3, while for distances greater than 20 mm the ratio was approximately 10^1.

The plastic work rate density, $\dot{W}^p(x_1, x_2) = \sigma_{ij}\dot{\varepsilon}_{ij}^p$, was then obtained from (3) for all specimens assuming $f = 0.9$.

Typical results are presented in Figs 20 and 21 which show the plastic work rate density distribution for specimen 9. Figure 20 shows contours of plastic work rate density. The maximum value of the plastic work rate density was 600×10^{12} J/m^3-s. It is seen that the active plastic zone (region where $\dot{W}^p > 0$) is situated just ahead of the crack tip and is elongated in the x_1 direction. This elongation was unexpected and must be related to the way the fracture meets the specimen surface along a 45° angle (see Fig. 17). Contours of plastic work rate farther from the crack tip are shown in Fig. 21. The distribution of $\dot{W}^p$ is very symmetric for this particular experiment. Note that in differentiating experimental data unavoidable numerical errors are introduced, hence little significance should be attributed to very low values of $\dot{W}^p$ that are below the noise level of the differentiation process which is on the order of 50×10^{12} J/m^3-s. The peak of $\dot{W}^p$ which lies ahead of the crack tip is clearly seen in Fig. 22 where $\dot{W}^p$ is plotted three dimensionally. This figure shows that except for a few oscillations, $\dot{W}^p$ is essentially zero everywhere except in a region just ahead of the crack tip.

A rough estimate of the norm of the plastic strain rate density at a distance of approximately 100 μm from the crack tip may be obtained from a simple calculation that assumes a von Mises yield criterion with a constant yield stress σ_0 equal to the

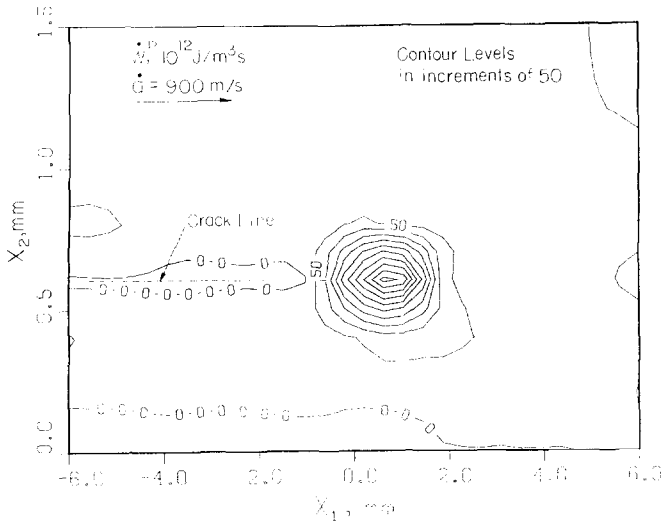

FIG. 21. Specimen 9. Contours of plastic work rate density away from crack tip. Increment between contours is 25×10^{12} J/m^3-s.

static value given in Table 1 for the quenched and tempered steel. In this case

$$\|\dot{\varepsilon}^p(\mathbf{x})\| = \frac{\dot{W}^p(\mathbf{x})}{\sigma_0}\sqrt{\frac{3}{2}}. \tag{4}$$

By using the maximum value of the plastic work rate density, $\dot{W}^p_{\max} = 600 \times 10^{12}$ J/m^3-s, (4) gives maximum strain rate $\|\dot{\varepsilon}^p\|_{\max} \simeq 7 \times 10^5$ s^{-1}. It should be noted that

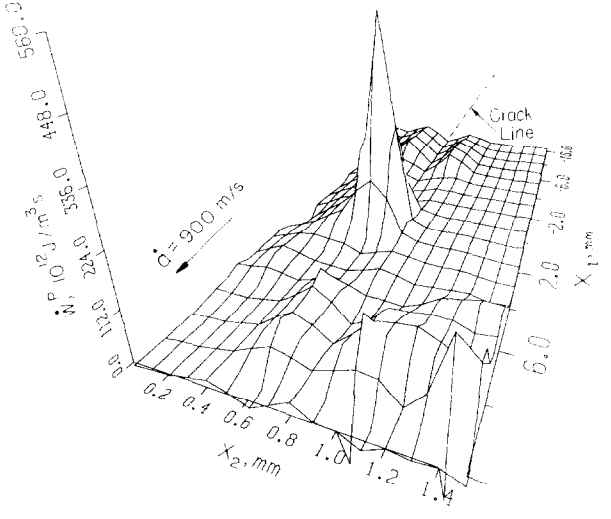

FIG. 22. Specimen 9. Surface plot of plastic work rate density.

this value of $\|\dot{\varepsilon}^p\|_{\max}$ corresponds to a distance of approximately 100 μm from the crack tip which is half of the distance between the centers of our measuring areas.

Comparison to Analytical Results

The temperature contours obtained here are very similar in shape to those calculated by Weichert and Schönert (1974) and Kuang and Atluri (1985). However, the values of temperature are quite different and cannot be compared since their calculation is intended to model brittle fracture where a high temperature localized over a very small region is expected. Rice and Levy (1969) modelled crack growth in elastic–plastic, rate insensitive materials and give an analytical relation for the maximum crack tip temperature rise which involves K_I^d, σ_0, $\dot{a}$ and the thermal properties of the material.

During crack growth K_I^d can be assumed to be equal to the dynamic fracture toughness K_{Ic}^d of the material. For the quenched and tempered 4340 steel, the K_{Ic}^d versus $\dot{a}$ relationships can be inferred from the experimental results of Zehnder and Rosakis (1989). For specimen 5 $\dot{a} = 980$ m/s and $K_{Ic}^d \approx 120$ MPa$\sqrt{m}$. Using these values, the thermal properties given in Table 1, and $\sigma_0 = 1490$ MPa, a temperature increase of 3800°C is predicted.

Although the peak measured temperatures are lower than the actual temperatures due to the averaging effect of the detector size, clearly the actual temperature rise is much lower than predicted. As discussed by Rice and Levy (1969), this is to be expected, since the Dugdale model used for their calculation lumps all of the deformation and hence all of the heating onto a single line.

Energy Fraction Absorbed in the Formation of Shear Lips During Dynamic Fracture

In this section we present a simple energy balance type of calculation designed to investigate the role of dynamic shear lip formation on the dissipation of energy during rapid crack growth. For this we will employ a recent result obtained by Freund and Hutchinson (1985) pertaining to steady-state dynamic crack growth in elastic–plastic solids under conditions of small-scale yielding. This result, which is presented here for the special case of *rate insensitive* elastic–plastic solids, states that the far field energy release rate G is given (in their notation) by

$$G = \int_{A_p} \sigma_{ij} \dot{\varepsilon}_{ij}^p(x_1, x_2)\, dA + \int_{-t}^{t} U_e^*(x_2)\, dx_2. \tag{5}$$

The first integral of the right-hand side of (5) is an area integral of the plastic work rate density $\dot{W}^p = \sigma_{ij}\dot{\varepsilon}_{ij}^p$ evaluated over the active plastic zone A_p (see Fig. 1). The second integral is evaluated over the width $(2t)$ of the plastic wake as $x_1 \to -\infty$ and involves the energy density due to residual elastic strains, $U_e^*(x_2)$, locked in this wake

after the passage of the crack, again as $x_1 \to -\infty$. Freund and Hutchinson show that the second term in the right-hand side of (5) is small compared to the first.

Also, for plane-stress *small-scale yielding* conditions, $G = \hat{f}(\dot{a}/c_r)\ (K_I^d)^2/E$, where K_I^d is the dynamic stress intensity factor, E is Young's modulus and $\hat{f}(\cdot)$ is a universally known function of crack tip velocity. As a result, an approximate form of (5) under plane stress conditions could be expressed as:

$$h\hat{f}\left(\frac{\dot{a}}{c_r}\right)\frac{(K_I^d)^2}{E} \cong h\int_{A_p} \dot{W}^p \, dA. \tag{6}$$

In the above,

$$h\hat{f}\left(\frac{\dot{a}}{c_r}\right)\frac{(K_I^d)^2}{E}$$

represents the energy per unit crack advance supplied to a crack in a specimen of thickness h by the far field, under small-scale yielding conditions, while the right-hand side is the energy per unit crack advance dissipated during plastic deformation.

Relation (6) strictly holds for two-dimensional plane stress, crack growth, and will have to be modified for application to cracks in real plate laboratory specimens where near tip three-dimensionality is evident through the formation of well-defined shear lips. The left-hand side of (6) need not be modified, since according to the small scale yielding assumption the dynamic stress intensity factor field K_I^d is operative far away from the crack tip where plane stress-type conditions exist in plate laboratory specimens of uniform thickness. This is however not true for the right-hand side, which involves integrals evaluated over the active plastic zone at distances from the crack tip that will almost certainly be affected by the near tip three-dimensional nature of the deformation state in a real (3-D) specimen. The right-hand side is therefore modified here by making the following simplifying assumptions. We first assume that near the specimen surface and through the thickness of the shear lip, h_s, both $\dot{W}^p$ and A_p remain uniform and can be provided by surface temperature measurement as described in a previous section, while we denote by R the thickness average of $\int \dot{W}^p \, dA$ through the specimen *interior*. Thus (6) becomes:

$$\hat{f}(\dot{a}/c_r)\frac{(K_I^d)^2}{E} \cong \frac{2h_s}{h}\int_{A_p} \dot{W}^p \, dA + \frac{(h-2h_s)}{h} R. \tag{7}$$

In the above expression the left-hand side can be evaluated from our experimental measurement of crack tip velocity, $\dot{a}$, as follows: For dynamic crack growth at velocity $\dot{a}$, the instantaneous value of the dynamic stress intensity factor K_I^d should be equal to the dynamic fracture toughness of the material, $K_{Ic}^d(\dot{a})$, which is a unique material dependent function of crack tip velocity. For one of the two treatments of 4340 steel investigated here (see "Quenched and Tempered Heat Treatment" of Table 1), $K_{Ic}(\dot{a})$ has been experimentally determined by ZEHNDER and ROSAKIS (1989), while $\hat{f}(\dot{a}/c_r)$ is a known function of $\dot{a}$ (see FREUND and HUTCHINSON, 1985). In the right-hand side of (7), the second term is unknown. This term represents the amount of available energy per unit crack advance dissipated in the specimen *interior*. However, the first

term can be computed from the calculation of $\dot{W}^p$ obtained by the surface temperature measurement, presented in a previous section (see also Figs 20–22). This term represents the amount of available energy per unit crack advance dissipated in the formation of the shear lip.

Evaluation of the terms of (7) for data corresponding to cracks propagating at velocities in the range of 700–900 m/s in the "Quenched and Tempered" steel indicate that the first term of the right-hand side of (7) is 60–70% of the left-hand side. If this simplified calculation is to be taken seriously, the results imply that 60–70% of the energy available to the crack through the far field loading is dissipated in the formation of shear lips and only 40–30% is dissipated in the specimen interior.

This result is surprising given the small thickness, $h_s \sim 0.75$ mm, of the shear lips observed in this heat-treatment of 4340. Nevertheless, if it is accurate, it clearly shows that the formation of shear lips has a substantial effect in the elevation of crack growth resistance in plate specimens of even moderately ductile metals. It should be noted here that qualitatively similar conclusions have been reached in recent experimental investigations by GIOVANOLA *et al.* (1989a), and GIOVANOLA *et al.* (1989b).

ROLE OF HEATING ON FRACTURE TOUGHNESS

The experimental data show that temperature increases up to 465°C may occur at the tip of dynamically propagating cracks in 4340 steel, while the region of intense heating (from maximum temperature to 100°C) is shown to extend as much as a third of the active plastic zone size. Such high and rather extensive temperature increases may have a significant effect on dynamic fracture propagation toughness. Three interacting phenomena that might be affected by local crack tip heating are outlined below. These are the decrease in yield stress at higher temperatures, the change in the fracture mechanism, and the change in the local structure of the near tip fields.

Data from the *Metals Handbook* (1978) on yield stress versus temperature for the tempered 4340 steel indicate that the yield stress in tension at 450°C is 50% lower than that at room temperature. Dislocation motion is thermally activated and will be affected by local crack tip heating even on the short time scales of this process, since there is no delay-time associated with the effect of temperature increase on dislocation mobility. As a result, near the crack tip there is a possibility of a substantial decrease of yield stress due to local heating.

A reduced yield stress near the crack tip will cause a change in the crack tip stress and strain fields compared to the fields that would exist under isothermal conditions. If crack growth is governed by a local criterion such as the attainment of a critical strain or opening angle at some distance near the crack tip, the effect of temperature on the local deformation fields will affect the fracture toughness of the material. It is not clear whether such effects will enhance or degrade fracture toughness. In general, lower yield stress values are associated with higher fracture toughness. Although this is true for a limited temperature range, this cannot be extrapolated indefinitely, since, in limit as the temperature approaches the melting point, both σ_0 and the fracture toughness must eventually approach zero.

Data of CHI *et al.* (1987) show that dynamic fracture *initiation* toughness for the

tempered 4340 steel at 100°C is 50% higher than at room temperature. Care must be taken in extrapolating this data to apply to dynamic fracture *propagation* toughness since in performing high temperature fracture *initiation* tests the material will be held at a high temperature for some time, causing a certain amount of heat treating (a slow diffusion controlled process) of the material to occur. However, in dynamic crack growth experiments there is insufficient time for any diffusion of atoms to take place and thus no heat treating can occur.

Indeed, during dynamic crack growth, the only property of the material that can respond to the local change in temperature on the time scales of the process (order of μs) is the yield stress. If the rupture process proceeds by the nucleation growth and coalescence of voids in front of the crack tip then one can speculate that a dramatic reduction of yield stress inside the process zone may, for example, enhance the mechanism of shear band formation between coalescing voids and thus may reduce the dynamic fracture toughness.

In an attempt to predict fracture toughness for dynamic crack growth, isothermal models use fracture criteria implemented very near the crack tip. It is exactly in such regions (process zones) where the experimental data show temperature rises as high as 500°C. In light of the above observation, it appears that thermal effects should be incorporated in such models.

REFERENCES

BAKER, L. and OLIVER, D. E. 1986 *SPIE Vol.* 685, *Infrared Technology* XII, 23.

BEVER, M. B., HOLT, D. L. and TITCHENER, A. L. 1973 *Progr. Mater Sci* **17**.

BRYANT, J. D., MAKEL, D. D. and WILSDORF, G. F. H 1986 *Mat. Sci. Engng*, **77**, 85.

CARSLAW, H. S. and JAEGER, J. C. 1959 *Conduction of Heat in Solids*. Clarenden Press, Oxford.

CHI, Y. C., LEE, H. S. and DUFFY, J. 1989 *Mater. Sci. Engng*, to appear.

DENG, X. and ROSAKIS, A. J. 1989 Work in progress, California Institute of Technology.

DÖLL, W. 1973 *Engng Fracture Mech.* **5**, 259.

DUFFY, J. 1984 *Mechanics of Material Behavior* p. 75 (edited by G. J. DVORAK). Elsevier, Amsterdam.

FOX, P. G. and SORIA-RUIZ, J. 1970 *Proc. R. Soc. (Lond.)* **A317**, 79.

FREUND, L. B. and HUTCHINSON, J. W. 1985 *J. Mech. Phys. Solids* **33**, 169.

FULLER, K. N. G., FOX, P. G. and FIELD, J. E. 1975 *Proc. R. Soc. (Lond.)* **A341**, 537.

GIOVANOLA, J. H., KLOPP R. W., SHOCKEY, D. A. and WERNER, A. T. 1989A *Proc. Seventh Int. Conf. Fracture* (ICF7), University of Houston, March 1989.

GIOVANOLA, J. H., KLOPP, R. W. and SIMONS, J. W. 1989B *Proc. Oji Int. Seminar Dynamic Fracture*, Toyohashi, Japan, 1–4 August, 1989

HARTLEY, K. A., DUFFY, J. and HAWLEY, R. H. 1987 *J. Mech. Phys. Solids* **35**, 283.

HUDAK, S. J., DEXTER, R. D., AARON, V. D. and NAGY, A. Internal Report, Southwest Research Institute.

KLEMM, W.	1989	*Proc. ASME JSME Int. Pressure and Piping Conf*, 23–27 July, 1989, Honolulu, Hawaii.
KRAFFT, J. M. and IRWIN, J. R.	1964	*Fracture Tough. Test. Applic. ASTM STP 381.*
KRISHNAKUMAR, R., NARASIMHAN, R. and PRABHAKAR, O.	1989	*Int. J. Fracture*, submitted.
KUANG, Z.-B. and ATLURI, S.	1985	*J. appl. Mech.* **52,** 277.
MALALI, P. N.	1988	Thermal fields generated by dynamic mode III fracture in ductile materials, M.S. Thesis, The Johns Hopkins University, Baltimore.
METALS HANDBOOK	1978	*Properties and Selection: Irons and Steels*, **1**. American Society for Metals.
MONCHALIN, J.	1984	*Nondestructive Methods for Material Property Determination*, p. 284 (edited by RUUD and GREEN). Plenum Press, New York.
MOSS, G. L. and POND, R. B.	1975	*Metall. Trans.* **6A,** 1223.
RICE, J. R. and LEVY, N.	1969	*Phys. Strength Plasticity*, p. 277.
SHOCKEY, D. A., KALTHOFF, J. F., KLEMM, S. and WINKLER, S.	1983	*Exper. Mech.* **40,** 140.
SUNG, J. C., and ACHENBACH, J. D.	1987	*J. Thermal Stresses* **10,** 243.
TAYLOR, G. I. and QUINNEY, M. A.	1934	*Proc. R. Soc.* **A143,** 307.
TOMASHEVSKII, E. E., EGOROV, E. A. and SAVOSTIN, A. YA.	1975	*Int. J. Fracture* **11,** 817.
WEICHERT, R. and SCHÖNERT, K.	1978	*J. Mech. Phys. Solids* **26,** 151.
ZEHNDER, A. T. and ROSAKIS, A. J.	1989	*Int. J. Fracture* to appear, Caltech Report, SM 86-6.